Electronic Supporting Information

Alchemical transformation method

Alchemical MD simulations have been performed using the simulation setup described in the main text (number of water molecules, force field, temperature, pressure, setup for Lennard-Jones and electrostatic interactions, time step, etc.). Using this methodology, the binding free energy of the macrocycle-anion system can be computed through a thermodynamic cycle as follows:[1]

$$\Delta G^\circ = \Delta G_2^\circ - \Delta G_1^\circ \quad (1)$$

Where ΔG_2° is the hydration free energy of the anion and ΔG_1° is the free energy for decoupling the anion from the rest of the system (macrocycle and solvent). In the present context, the term "decoupled molecule" is used to indicate a state in which all interactions of the molecule with the rest of the system are switched off. To compute ΔG_1°, we have used the single-point alchemical-path scheme introduced in Refs. 1 and 2. In this approach, we need to identify a coordinate for defining the position of the anion relative to the macrocycle. Here, we adopt the distance r between the anion (P and S atoms in the cases of $H_2PO_4^-$ and SO_4^{2-} anions) and the centroid defined by the atoms of the H_4L^{4+}/H_5L^{5+} moiety (specifically, the C and N atoms of the aromatic condensed rings). Then, a specific value of r, say r', must be chosen to identify a generic bound state of the system. The choice of an optimal r' is not mandatory, provided that r' represents the bound state satisfactorily (according to chemical intuition). We have chosen $r' = 4$ Å. Once r' is defined, the decoupling free energy ΔG_1° is computed as

$$\Delta G_1^\circ = \phi(1, r') - \phi(0, r') - RT \ln\left(\frac{\rho(r')}{C^\circ}\right) \quad (2)$$

where $\rho(r')$ is the probability density of finding the system in a configuration $r = r'$ during an equilibrium MD simulation of the bounded state, $\phi(1, r')$ is the potential of mean force of a configuration with $r = r'$ and the anion decoupled from the rest of the system and $\phi(0, r')$ is the potential of mean force with all the potential in place. Finally, C° is the standard concentration (1 M or 1 molecule / 1661 Å^3), R the ideal gas constant and T the absolute temperature. We have calculated $\rho(r')$ from standard MD simulations of the bounded state of the macrocycle-anion complexes. In particular, we performed a simulation lasting 5 ns. Evaluation of the quantity $\phi(1, r') - \phi(0, r')$ has been done through nonequilibrium simulations during which the anion has been decoupled from the rest of the system, namely macrocycle and solvent. The initial microstates have been sampled from an equilibrium simulation of the fully coupled system, enforcing a stiff harmonic restraint of type $U(r) = k(r - r')^2$. The equilibrium distance is clearly $r' = 4$ Å, while the force constant k is 1000 kcal mol^{-1} Å^{-2}. For all systems, 500 microstates (atomic coordinates and velocities) have been stored at regular time intervals of 3 ps, after an equilibration phase of 2 ns. Starting from the saved microstates, nonequilibrium alchemical trajectories of 120 ps have been realized. During each trajectory, the interaction potential of the anion with the rest of the system is externally modulated under an established linear protocol, leading the system from the coupled to the uncoupled state, while leaving in place the restraining potential $U(r)$. In particular, all nonequilibrium alchemical trajectories have been realized by switching off the electrostatic interactions in the first half of the run, that is, from 0 to 60 ps, while the Lennard-Jones interactions have been switched off in the second half of the run, from 60 to 120 ps. The functional form of the switched interaction potential is in accord with that of Ref. 3. During each decoupling simulation, the nonequilibrium work W is

computed thus obtaining 500 sampled work values. This set of values has finally been used in the Jarzynski relationship[4] to obtain $\phi(1,r') - \phi(0,r')$:

$$\phi(1,r') - \phi(0,r') = -RT \ln\langle \exp(-W/(RT)) \rangle \quad (3)$$

where the exponential average $\langle \cdots \rangle$ is evaluated using the 500 work samples. To calculate the hydration free energy ΔG_2° entering eq. 1, alchemical MD simulations of the only decoupling process of the solvated anion have been realized. Initial microstates are sampled from an equilibrium simulation of the anion in aqueous solution, without enforcing any restraint to the anion. A total of 500 microstates were stored every 3 ps. The functional form of the switched interaction potential, as well as the time schedule for the alchemical parameter, are equal to those applied in the alchemical trajectories described above. Then nonequilibrium decoupling simulations have been carried out to get 500 work samples, eventually employed in the Jarzynski relationship (eq. 3) to get the opposite of ΔG_2°. We finally point out that changes in volume upon decoupling have been disregarded in the calculation, because constant-pressure constant-temperature equations of motion are employed.

Flexibility of the alkyl chain: the root mean square displacement

The root mean square displacement (RMSD) for a given configuration of the macrocycle picked from the MD simulation is defined considering the experimental structure as the reference one. Denoting the vector position of an atom i of the simulated structure at time t as $\boldsymbol{r}_{i,t,\mathrm{MD}}$ and the vector position of the same atom in experimental structure as $\boldsymbol{r}_{i,\mathrm{exp}}$, then the RMSD for the configuration t is defined as

$$\mathrm{RMSD}(t) = \sqrt{1/N \sum_{i=1}^{N} \left| \boldsymbol{r}_{i,t,\mathrm{MD}} - \boldsymbol{r}_{i,\mathrm{exp}} \right|^2} \quad (4)$$

where the sum runs over all the atoms of interest. In our case, as we want to evaluate the flexibility of the alkyl chain of the macrocycle, the atoms of interest are all the N and C atoms of the alkyl chain (the atoms of the condensed aromatic rings are excluded). It is important to note that, before applying eq. 4, the macrocycle configuration obtained from the simulation is roto-translated so as to overlap the three condensed aromatic rings with the experimental ones. Here, the optimal overlap is obtained by minimizing the RMSD computed over the C and N atoms of the aromatic rings. The RMSD computed from MD simulations of various complexes is reported in the Figures S2 and S3.

Geometrical criteria to identify the poses of the complexes

The populations of the various poses observed during the MD simulations of the complexes and reported in the Figures 8-11 of the main text have been roughly estimated by simply counting the number of times the anion (or the P and S atoms in the case of $H_2PO_4^-$ and SO_4^{2-}) is found in established R and θ ranges, where R is the distance of the anion (or the P and S atoms) from the centroid of the three aromatic rings and θ is the angle formed by the vector position of the anion (or the P and S atoms), relative to the centroid of the aromatic rings, and the normal to the aromatic rings. Given a system with two poses, say, *A* and *B*, counted n_A and n_B times during the simulation run, the percentage populations are $100\, n_A/(n_A + n_B)$ and $100\, n_B/(n_A + n_B)$. In Tables S8 and S9, we report the R and θ ranges employed for the various poses related to the complex in the tetra- and pentaprotonated forms, respectively.

References

1. Giovannelli, E.; Procacci, P.; Cardini, G.; Pagliai, M.; Volkov, V.; Chelli R. Binding free energies of host-guest systems by nonequilibrium alchemical simulations with constrained dynamics: Theoretical framework.
J. Chem. Theory Comput. 2017, 13, 5874-5886.

2. Giovannelli, E.; Cioni, M.; Procacci, P.; Cardini, G.; Pagliai, M.; Volkov, V.; Chelli R. Binding free energies of host-guest systems by nonequilibrium alchemical simulations with constrained dynamics: Illustrative calculations and numerical validation.
J. Chem. Theory Comput. 2017, 13, 5887-5899.

3. Procacci, P.; Cardelli, C. Fast switching alchemical transformations in molecular dynamics simulations.
J. Chem. Theory Comput. 2014, 10, 2813-2823.

4. Jarzynski, C. Nonequilibrium equality for free energy differences.
Phys. Rev. Lett. 1997, 78, 2690-2693.

Table S1. Crystal data and refinement parameters for $H_5LCl_5 \cdot 4H_2O$ (**1**) (a), $H_5LBr_5 \cdot 4H_2O$ (**2**) (b), $H_5L(NO_3)_5 \cdot 3H_2O$ (**3**) (c), $H_5L(H_2PO_4)_5 \cdot (H_3PO_4)_2 \cdot 4H_2O$ (**4**).

	(**1**)	(**2**)	(**3**)	(**4**)
Empirical formula	$C_{24}H_{46}Cl_5N_5O_4$	$C_{24}H_{46}Br_5N_5O_4$	$C_{24}H_{44}N_{10}O_{18}$	$C_{24}H_{62}N_5O_{32}P_7$
Formula weight	645.91	868.21	760.69	1149.57
Temperature (K)	293	293	293	293
Crystal system	triclinic	triclinic	triclinic	triclinic
space group	*P*-1	*P*-1	*P*-1	*P*-1
a (Å)	7.688(1)	7.806(1)	7.664(1)	11.961(2)
b (Å)	13.744(2)	13.978(1)	11.930(1)	13.583(2)
c (Å)	15.732(2)	16.174(2)	19.291(2)	15.357(2)
α (°)	80.34(1)	80.313(8)	78.898(9)	85.66(1)
β (°)	79.66(1)	78.81(1)	82.80(1)	75.95(1)
γ (°)	79.50(1)	78.280(9)	87.09(1)	69.72(1)
Volume ($Å^3$)	1592.1(4)	1679.8(3)	1716.5(3)	2270.2(6)
Z	2	2	2	2
Independent reflections / R(int)	3096/ 0.0679	3257/ 0.0946	3329/ 0.0352	5767/ 0.0650
μ (mm^{-1})	4.455 (Cu-Kα)	7.533 (Cu-Kα)	1.094 (Cu-Kα)	3.520 (Cu-Kα)
R indices [I>2σ(I)][a]	R1 =0.0523	R1 =0.0552	R1 =0.0 944	R1 = 0.0740
	wR2 = 0.1428	wR2 =0.1471	wR2 =0. 2592	wR2 =0.1821
R indices (all data)[a]	R1 =0.0791	R1 = 0.0711	R1 =0. 1530	R1 =0.1491
	wR2 = 0.1594	wR2 =0.1609	wR2 =0. 2906	wR2 =0.2009

[a] $R1 = \Sigma \, | \, |Fo| - |Fc| \, | \, / \Sigma \, |Fo|$; $wR2 = [\, \Sigma \, w(Fo^2 - Fc^2)^2 \, / \, \Sigma \, wF$

Table S2. H-bond contacts in the crystal structure of **1**

	d (Å)	D-H-A (deg)	Symmetry operator to be applied to the second atom
N2···Cl1	3.075(5)	163.0(3)	
N2···Cl5	3.019(5)	165.5(3)	
N3···Cl2	3.150(5)	172.0(3)	
N5···Cl4	3.089(5)	171.4(3)	
N3···Cl3	3.157(5)	157.7(3)	
N1···Cl2	3.123(5)	168.2(3)	-x+1,-y+1,-z+2
N5···Cl1	3.148(4)	160.2(3)	x-1,+y+1,+z
N4···OW3	2.821(7)	161.3(3)	
N4···OW1	2.781(6)	167.0(3)	
Cl2···OW1	3.175(4)		
Cl4···OW1	3.102(4)		
Cl1···OW2	3.128(4)		-x+2,-y+1,-z+1
Cl3···OW2	3.227(5)		-x+2,-y+1,-z+1
Cl3···OW3	3.241(5)		x+1, +y,+z
Cl5···OW1	3.858(4)		x,+y-1,+z
Cl5···OW4	3.882(6)		x,+y-1,+z
Cl5···OW4	3.103(6)		-x+2,-y+1,-z+1
OW2···OW4	2.897(8)		
OW3···OW4	2.725(7)		x-1,+y,+z

Table S3 – H-bond contacts in the crystal structure of **2**

	d (Å)	D-H-A (deg)	Symmetry operator to be applied to the second atom
N2···Br5	3.185(8)	164.7(5)	
N3···Br3	3.296(8)	169.1(5)	
N3···Br2	3.286(8)	151.5(6)	
N5···Br1	3.293(7)	156.6(5)	
N5···Br4	3.258(9)	171.5(5)	
N1···Br3	3.307(9)	169.6(5)	-x+1,-y,-z+1
N2···Br1	3.220(9)	166.1(5)	x+1,+y-1,+z
N4···OW1	2.85(1)	159.7(6)	
N4···OW4	2.80(1)	167.9(6)	
Br1···OW2	3.265(7)		
Br3···OW4	3.300(7)		
Br4···OW4	3.248(7)		
OW1···OW3	2.71(1)		
OW1···Br2	3.365(8)		x-1,+y,+z
OW2···Br2	3.370(8)		x-1,+y+1,+z
OW2···OW3	2.82(2)		-x,-y+1,-z
OW3···Br5	3.96(1)		x-1,+y+1,+z
OW3···Br5	3.27(1)		-x+1,-y,-z
OW3···OW2	2.82(2)		-x,-y+1,-z
OW4···Br5	3.921(7)		x,+y+1,+z

Table S4. H-bond contacts in the crystal structure of **3**

	d (Å)	D-H-A (deg)	Symmetry operator to be applied to the second atom
N2···O71	2.95(1)	149.8(5)	
N2···O72	3.02(1)	150.7(5)	
N4···O81	2.78(1)	169.8(6)	
N4···O61	2.99(1)	152.2(5)	
N5···O103	2.859(9)	175.8(4)	
N5···O92	2.80(1)	169.5(4)	
N1···O101	2.907(9)	156.6(5)	x,+y+1,+z
N2···OW1	2.79(1)	171.2(5)	
N3···OW3	2.88(1)	152.2(5)	
N3···OW2	2.77(1)	167.8(5)	
O61···OW2	3.10(1)		
O61···OW3	3.15(1)		
O62···OW3	2.81(1)		
OW1···OW3	3.29(1)		
OW2···OW3	3.98(1)		
OW1···O71	2.84(1)		x+1,+y,+z
OW1···O82	2.81(1)		x-1,+y+1,+z
OW1···O83	2.98(1)		x-1,+y+1,+z
OW2···O63	2.78(1)		x-1,+y,+z
OW2···O91	2.68(1)		x-1,+y,+z
OW3···O72	3.29(1)		-x,-y,-z+1

Table S5. H-bond contacts in the crystal structure of **4**

	d (Å)	D-H-A (deg)	Symmetry operator to be applied to the second atom
N1···O63	2.654(9)	176.9(5)	
N2···O22	2.86(1)	161.4(5)	
N5···O42	2.841(8)	162.7(5)	
N5···O73	2.73(2)	159.8(6)	
N3···O33	2.839(7)	161.2(5)	
N4···O13	2.800(8)	176.3(5)	
N4···O52	2.81(1)	162.7(6)	
N2···O23	2.822(7)	143.4(5)	-x+2,-y,-z-1
N3···O12	2.830(8)	173.0(4)	-x+2,-y,-z
O14···O43	2.616(7)		
O31···OW1	2.84(1)		
O54···OW4	2.44(2)		
O11···O12	2.556(7)		-x+2,-y,-z
O13···O23	2.508(9)		x,+y,+z+1
O21···O51	2.561(8)		x,+y,+z-1
O21···OW2	2.95(1)		x,+y,+z-1
O24···O44	2.482(7)		-x+2,-y,-z
O24···OW3	2.75(2)		x,+y,+z-1
O22···O42	2.46(1)		x,+y,+z-1
O34···O53	2.52(1)		-x+2,-y+1,-z
O33···O32	2.531(8)		-x+1,-y+1,-z
O31···O61	2.35(2)		-x+1,-y,-z
O41···O41	2.461(7)		-x+1,-y,-z+1
O43···O76	2.53(2)		-x+1,-y,-z+1
O43···O75	2.48(2)		-x+1,-y,-z+1
O51···O21	2.561(8)		x,+y,+z+1
O52···O64	2.52(1)		x,+y+1,+z
O53···O62	2.44(1)		-x+2,-y,-z
O61···O77	2.51(3)		-x+1,-y,-z+1
O71···OW2	3.11(2)		-x+1,-y+1,-z+1
O76···O43	2.53(2)		-x+1,-y,-z+1
O73···OW1	2.92(2)		x,+y,+z+1
O73···OW2	2.77(2)		-x+1,-y+1,-z+1
O77···O61	2.51(3)		-x+1,-y,-z+1
O77···OW1	3.27(2)		x,+y,+z+1
O72···OW2	2.74(2)		-x+1,-y+1,-z+1
O72···OW3	2.75(2)		x-1,+y,+z
O72···OW4	2.57(3)		x-1,+y,+z
O74···OW1	2.49(3)		x,+y,+z+1
O75···O43	2.48(2)		-x+1,-y,-z+1
O75···OW3	2.91(3)		x-1,+y,+z
OW1···O61	3.95(1)		-x+1,-y,-z
OW1···OW2	2.75(1)		x,+y,+z-1
OW2···OW4	2.79(3)		-x+2,-y+1,-z+1
OW3···OW4	2.92(2)		-x+2,-y+1,-z+1

Table S6. H_5L^{5+} Hirshfeld surface percent composition in compounds **1** and **2**.

Inside Atom	*Outside Atom*					
	Cl	***N***	***H***	***C***	***O***	***Total***
C	1.7	0.5	3.4	4.3	0.1	9.9
Cl	.	.	.	.	.	0.0
H	33.6	0.1	30.0	2.6	22.8	89.2
N	0.2	.	0.3	0.4	.	0.9
O	.	.	.	.	.	0.0
Total	35.5	0.6	33.7	7.4	22.9	

Inside Atom	*Outside Atom*					
	Br	***N***	***H***	***C***	***O***	***Total***
Br	.	.	.	.	.	0.0
C	1.8	0.4	3.5	4.1	0.1	9.9
H	35.4	0.0	27.6	2.6	23.6	89.2
N	0.2	.	0.2	0.4	.	0.9
O	.	.	.	.	.	0.0
Total	37.5	0.5	31.2	7.2	23.7	

Table S7. Calculated and experimental equilibrium constants of the complexes. The calculated values have been established according to the known relation between equilibrium constant and reaction free energy, $\Delta G^\circ = -RT \ln K$.

	Complexes with H_4L^{4+}		Complexes with H_5L^{5+}	
	log$K$ (calc.)	log$K$ (exp)	log$K$ (calc)	log$K$ (exp.)
F^-	2.1	4.4	5.3	5.2
Cl^-	2.4	3.8	3.8	4.7
Br^-	1.5	3.5	2.8	4.3
I^-	0.9	----	1.5	2.9
$H_2PO_4^-$	1.1	2.6	2.2	2.9
SO_4^{2-}	1.3	----	1.7	----

Table S8. Ranges for the R distance and θ angle adopted to define the poses of the complexes formed by the macrocycle in the H_4L^{4+} form. In the first column, the anion involved in the complex is reported.

Anion	Pose	R (Å)	θ (degrees)
F^-	A1	3.5 4.5	10 30
F^-	B	5.0 8.0	15 40
F^-	C	5.5 7.5	50 75
Cl^-	A	3.5 5.0	15 35
Cl^-	B	5.0 6.5	60 85
$H_2PO_4^-$	A2	4.5 6.0	25 40
$H_2PO_4^-$	B2	6.5 8.5	55 90
$H_2PO_4^-$	C2	7.0 8.0	10 40
SO_4^{2-}	A	6.0 9.0	10 40

Table S9. Ranges for the R distance and θ angle adopted to define the poses of the complexes formed by the macrocycle in the H_5L^{5+} form. In the first column, the anion involved in the complex is reported.

Anion	Pose	R (Å)	θ (degrees)
F^-	A2	3.0 4.5	10 35
F^-	B	5.5 7.5	15 35
F^-	C	5.5 7.5	50 75
Cl^-	A	3.5 5.0	10 35
Cl^-	B	4.5 6.5	60 90
Br^-	A	3.5 5.0	10 35
Br^-	B	5.0 6.0	65 85
I^-	A	4.0 5.0	15 35
I^-	B	5.0 6.5	65 90
$H_2PO_4^-$	A1	3.8 5.0	15 40
$H_2PO_4^-$	B1	6.0 7.0	50 65
SO_4^{2-}	A	4.6 6.0	35 50
SO_4^{2-}	B	6.5 8.0	20 35
SO_4^{2-}	C	6.0 7.0	50 65

Table S10. AMBER atom-types and atomic net charges (obtained from a RESP fit at the HF/6-31G* level of theory) of chemically non-equivalent atoms of the H_4L^{4+} species. The atom labels refer to those displayed in Figure S5a.

Atom label	AMBER atom-type	Charge (e)
C1	**cb** (sp_2 aromatic C)	0.5826325
C2	**cb** (sp_2 aromatic C)	−0.102485
C3	**cb** (sp_2 aromatic C)	−0.115467
C4	**cb** (sp_2 aromatic C)	0.209435
C5	**cb** (sp_2 aromatic C)	−0.187675
C6	**cb** (sp_2 aromatic C)	−0.246825
C7	**ct** (sp_3 aliphatic C)	−0.262389
C8	**ct** (sp_3 aliphatic C)	0.0538445
C9	**ct** (sp_3 aliphatic C)	−0.0970585
C10	**ct** (sp_3 aliphatic C)	−0.036029
C11	**ct** (sp_3 aliphatic C)	−0.0001235
C12	**ct** (sp_3 aliphatic C)	−0.220219
N1	**nc** (sp_2 N in 6 memb. ring with lone pair)	−0.691306
N2	**nt** (sp_3 N for amino groups)	−0.3975315
N3	**nt** (sp_3 N for amino groups)	−0.278185
H1	**ha** (H arom. bond. to C without electrwd. groups)	0.138089
H2	**ha** (H arom. bond. to C without electrwd. groups)	0.117314
H3	**ha** (H arom. bond. to C without electrwd. groups)	0.181126
H4	**ha** (H arom. bond. to C without electrwd. groups)	0.214891
H5	**h1** (H aliph. bond. to C with 1 electrwd. group)	0.20238075
H6	**h** (H bonded to N)	0.3802315
H7	**h1** (H aliph. bond. to C with 1 electrwd. group)	0.06708
H8	**hc** (H aliph. bond. to C without electrwd. groups)	0.07990675
H9	**h1** (H aliph. bond. to C with 1 electrwd. group)	0.12755775
H10	**h** (H bonded to N)	0.34080725
H11	**h1** (H aliph. bond. to C with 1 electrwd. group)	0.1287435
H12	**hc** (H aliph. bond. to C without electrwd. groups)	0.1380485

Table S11. AMBER atom-types and atomic net charges (obtained from a RESP fit at the HF/6-31G* level of theory) of chemically non-equivalent atoms of the H_5L^{5+} species. The atom labels refer to those displayed in Figure S5b.

Atom label	AMBER atom-type	Charge (e)
C1	**cb** (sp_2 aromatic C)	0.067853
C2	**cb** (sp_2 aromatic C)	0.299417
C3	**cb** (sp_2 aromatic C)	−0.220544
C4	**cb** (sp_2 aromatic C)	0.2766505
C5	**cb** (sp_2 aromatic C)	−0.105931
C6	**cb** (sp_2 aromatic C)	−0.169553
C7	**ct** (sp_3 aliphatic C)	−0.29553
C8	**ct** (sp_3 aliphatic C)	0.0292175
C9	**ct** (sp_3 aliphatic C)	−0.086072
C10	**ct** (sp_3 aliphatic C)	−0.091194
C11	**ct** (sp_3 aliphatic C)	−0.110097
C12	**ct** (sp_3 aliphatic C)	−0.094870
N1	**nc** (sp_2 N in 6 memb. ring with lone pair)	−0.146397
N2	**nt** (sp_3 N for amino groups)	−0.422922
N3	**nt** (sp_3 N for amino groups)	−0.2477405
H1	**ha** (H arom. bond. to C without electrwd. groups)	0.215994
H2	**ha** (H arom. bond. to C without electrwd. groups)	0.1553605
H3	**ha** (H arom. bond. to C without electrwd. groups)	0.1961905
H4	**ha** (H arom. bond. to C without electrwd. groups)	0.217083
H5	**h1** (H aliph. bond. to C with 1 electrwd. group)	0.228113
H6	**h** (H bonded to N)	0.40155875
H7	**h1** (H aliph. bond. to C with 1 electrwd. group)	0.08162975
H8	**hc** (H aliph. bond. to C without electrwd.groups)	0.0851305
H9	**h1** (H aliph. bond. to C with 1 electrwd. group)	0.15115025
H10	**h** (H bonded N)	0.332749
H11	**h1** (H aliph. bond. to C with 1 electrwd. group)	0.162618
H12	**hc** (H aliph. bond. to C without electrwd. groups)	0.118768
H13	**h** (H bonded N)	0.348217

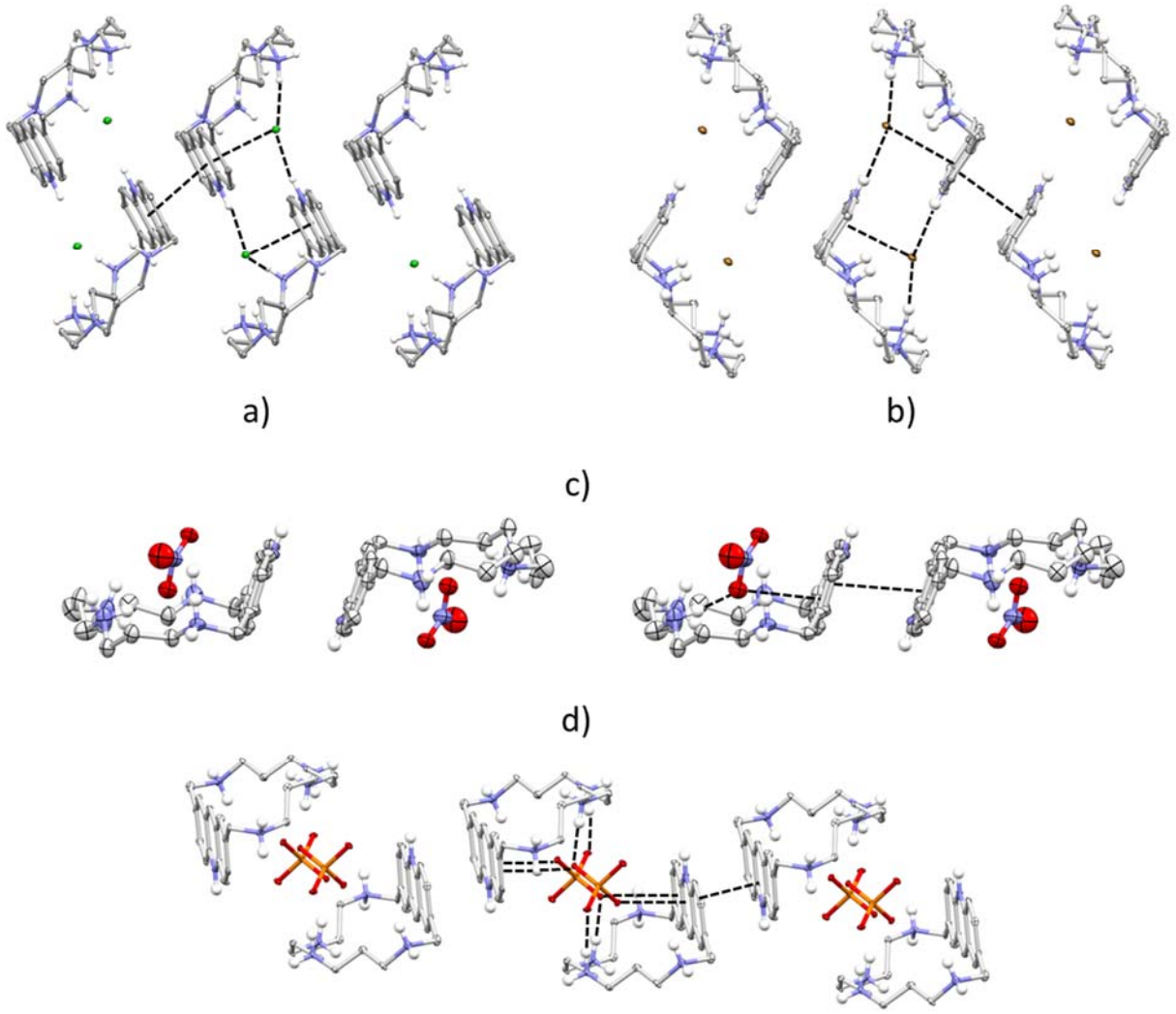

Figure S1. Details of the crystal packing of complexes **1**-**4** (a to d, respectively)

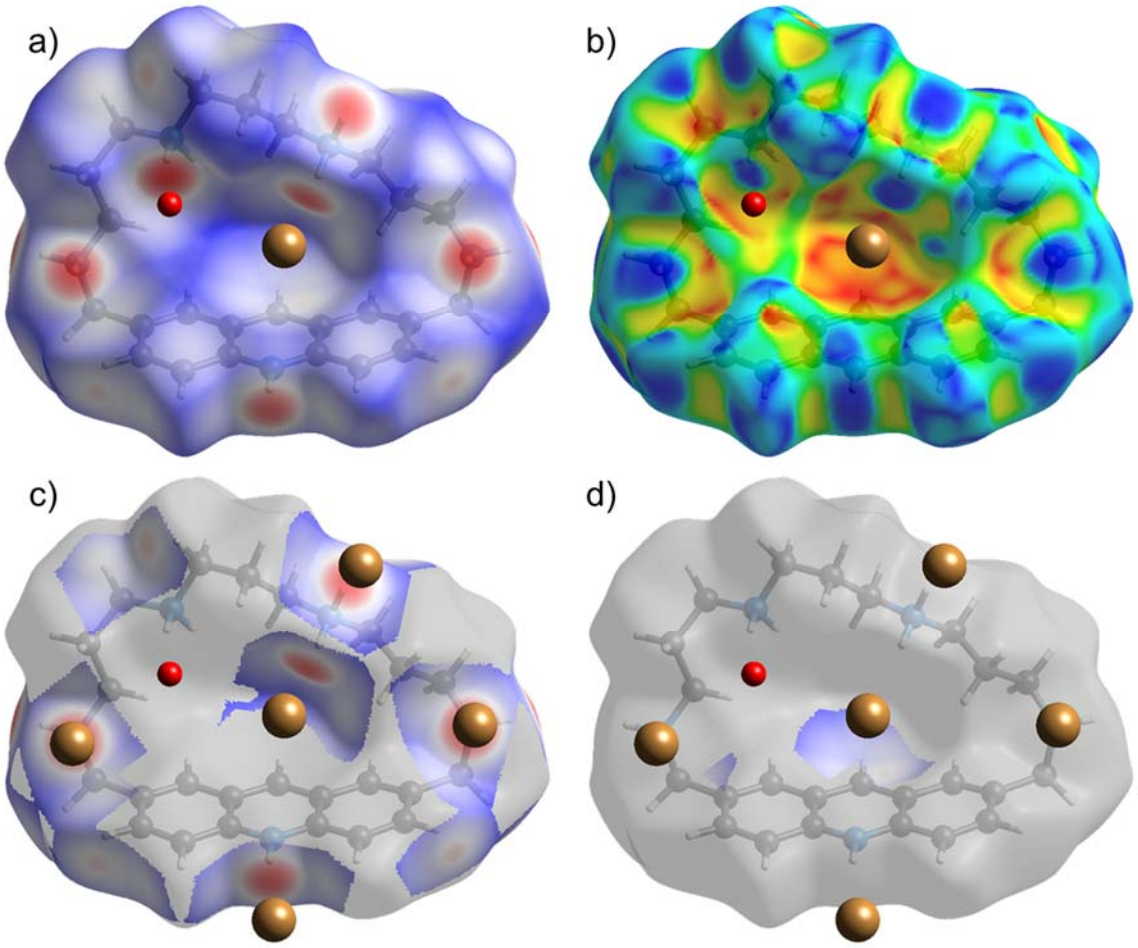

Figure S2. Ligand Hirshfeld surface in compound **2**. a) contact distance (d_{norm}) standard coloring. b) shape index coloring; c) visualization of H···Br contacts, corresponding to CH···anion (weak interactions) and $^{+}$NH···Br salt-bridges (red interaction hotspots, Br^{-} anions in contact shown); d) visualization of C···Br contacts (anion···π interactions) which highlight the involvement of the whole central heterocycle.

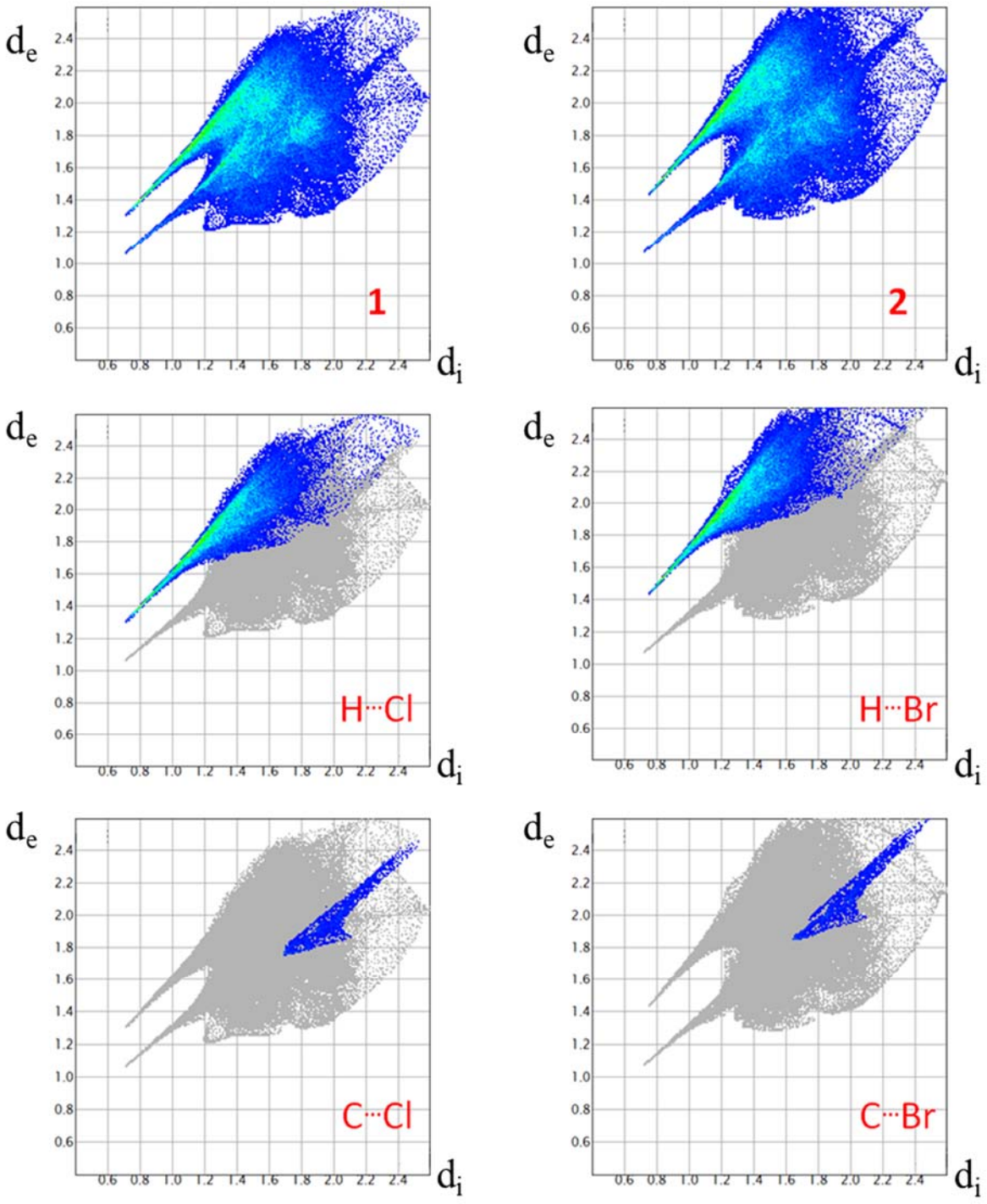

Figure S3. Plots of external *vs.* internal distances (d_e and d_i, respectively) from the Hirshfeld surface of H_5L^{5+} (fingerprint plots) in **1** and **2** (top), with details of H···anion contacts (middle) and C···anion contacts (anion-π interactions) (bottom).

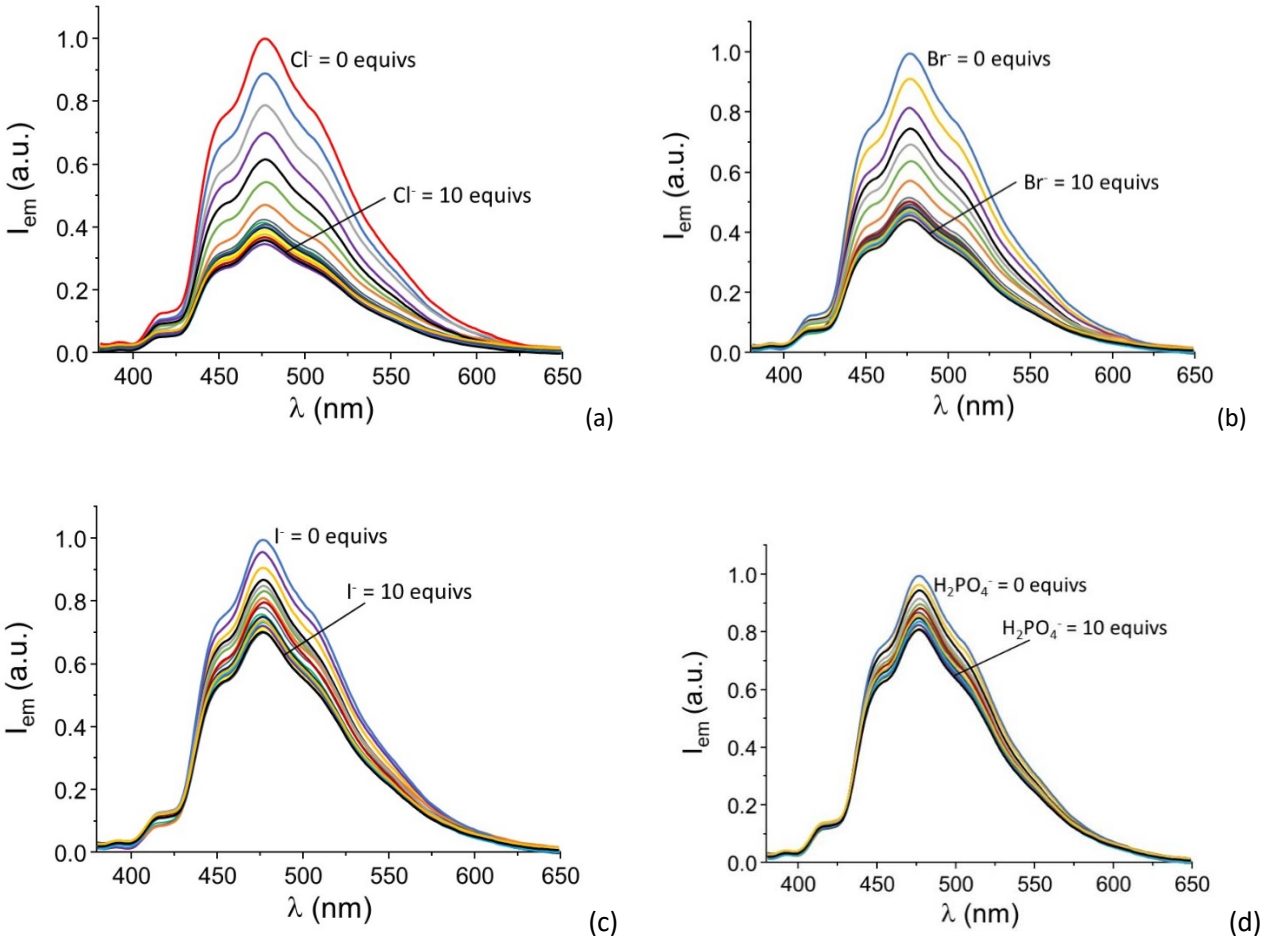

Figure S4. Emission spectra of **L** in the presence of increasing amounts (up to 10 equivs.) of Cl^- (a), Br^- (b), I^- (c) and $H_2PO_4^-$ (d) at pH 3.5 (T = 298 K, λ_{exc} = 370 nm).

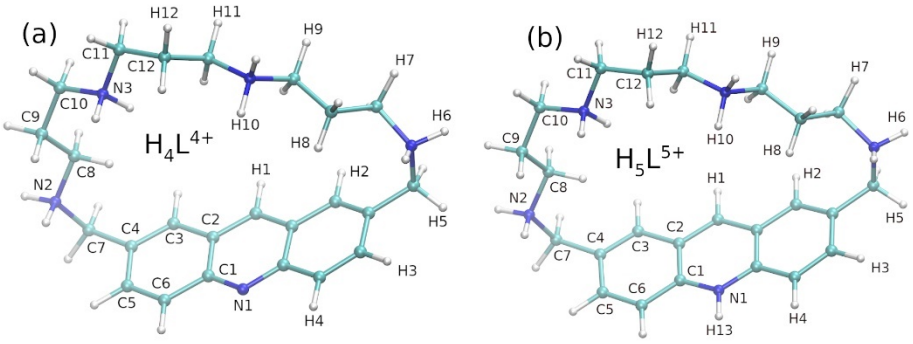

Figure S5. Ball and stick representations of the H_4L^{4+} (a) and H_5L^{5+} (b) species. Only the labels of chemically non-equivalent atoms are reported (cyan: C atoms; blue: N atoms; white: H atoms).

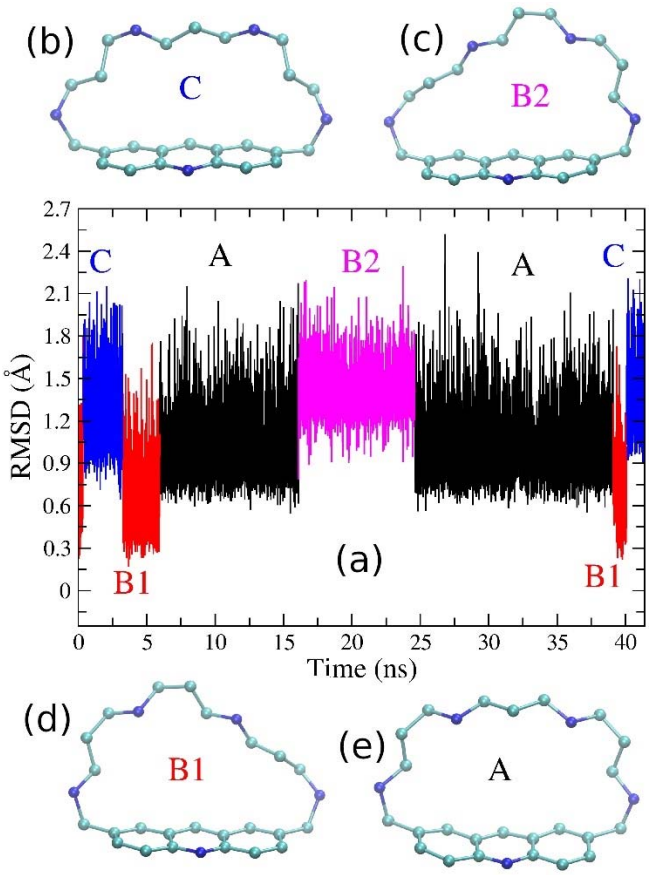

Figure S6. RMSD as a function of time calculated from a MD simulation of the $[H_4LCl]^{3+}$ complex (a). The conformational assignment is also reported (b, c, d and e).

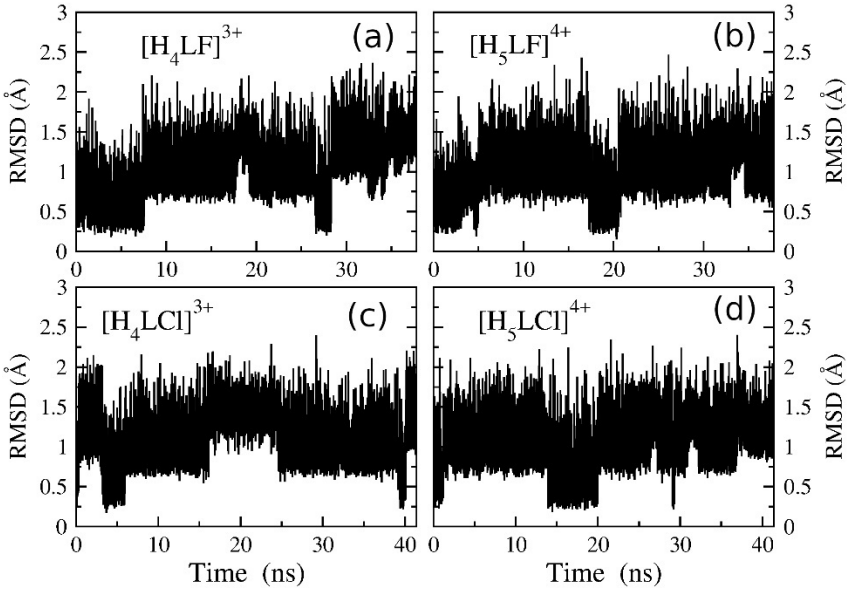

Figure S7. RMSD as a function of time calculated from MD simulations of the $[H_4LF]^{3+}$, $[H_5LF]^{4+}$, $[H_4LCl]^{3+}$ (also reported in Figure S6) and $[H_5LCl]^{4+}$ complexes (a, b, c and d, respectively).

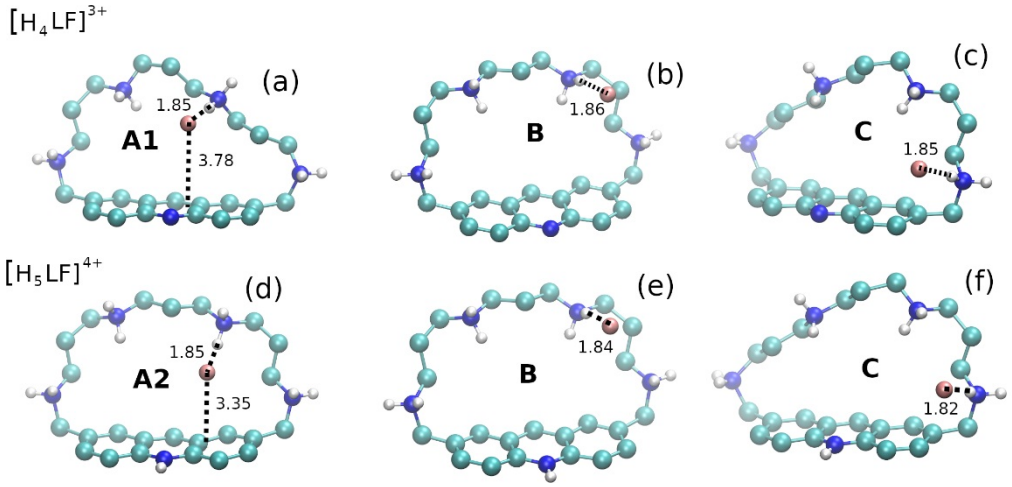

Figure S8. Ball and stick representations of the A1 (a), B (b) and C (c) poses related to the $[H_4LF]^{3+}$ complex and A2 (d), B (e) and C (f) poses related to the $[H_5LF]^{4+}$ complex, whose two-dimensional distribution functions of R and θ are displayed in Figure 8 of the main text. The representations are supplied with the relevant H-bond and anion-aromatic plane distances (in Å).

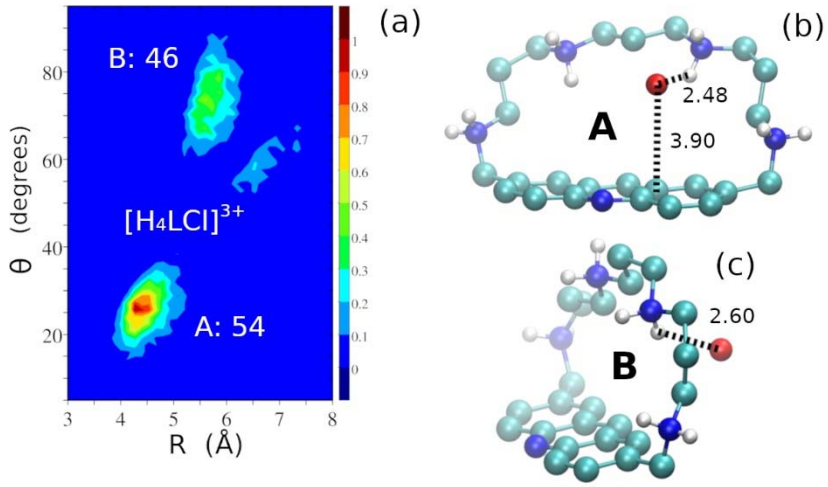

Figure S9. Two-dimensional distribution function of R and θ for the $[H_4LCl]^{3+}$ adduct (a). Ball and stick representations of the A (b) and B (c) poses are also displayed, highlighting the relevant H-bond and anion-aromatic plane distances (in Å). Populations are computed according to the geometrical definitions of the poses reported in Table S10 of the present report.

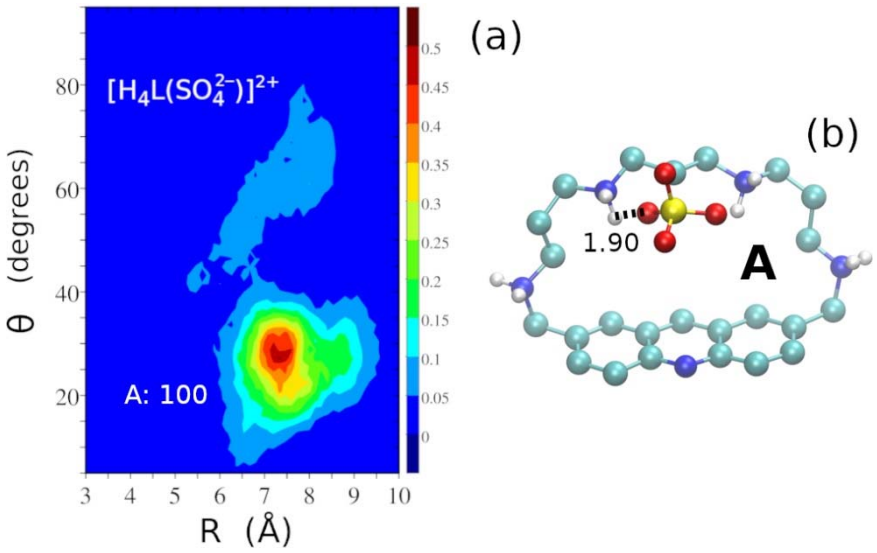

Figure S10. Two-dimensional distribution function of R and θ for the $[H_4L(SO_4)]^{2+}$ adduct (a). Ball and stick representation of the only A pose (b) is also displayed, highlighting the relevant H-bond distance (in Å).